Single-Model Single-Feedback Digital Predistortion for Concurrent Multi-band Wireless Transmitters

Chao Yu, *Member*, *IEEE*, Jing Xia, *Member*, *IEEE*, Xiao-Wei Zhu, *Member*, *IEEE*, and Anding Zhu, *Senior Member*, *IEEE*

***Abstract*—In this paper, a novel single-model single-feedback digital predistortion (DPD) technique is proposed to linearize concurrent multi-band wireless transmitters. By employing carrier relocation and band-limiting functions in digital signal processing, DPD model complexity is significantly reduced and only one narrow band feedback loop is required for data acquisition. In the new system, the linearization bandwidth can be arbitrarily reconfigured, which provides considerable flexibility for DPD system design in wideband concurrent operations. Experimental tests were conducted to validate various cases including a concurrent quad-band scenario that is reported for the first time to date. Excellent performance demonstrates that the proposed approach provides an effective solution for reducing DPD system implementation complexity and cost in both digital and analog domains for future wideband concurrent multi-band transmitters.**

***Index Terms*—concurrent, digital predistortion (DPD), linearization, multi-band, power amplifiers (PAs), wideband.**

I. Introduction

TO meet the ever increasing demands for high data rates and large network capacity, the modulation signal bandwidth of cellular base station transmitters is continuously increasing. Because most of the spectrum in the cellular bands have already been allocated, it is often difficult to find a single contiguous band to meet the wideband requirement. Carrier aggregation [1] has been proposed to aggregate multiple bands located at different carrier frequencies to conduct high speed data transmission. This requires concurrent multi-band transmitters to be deployed in wireless systems. Similar to single band transmitters, distortion introduced by radio frequency (RF) power amplifiers (PAs) in multi-band transmitters not only reduces the quality of the signal but also affects users in the adjacent channels.

Digital predistortion (DPD) is one of the advanced linearization techniques that compensates for nonlinear distortion of RF PAs by inverting their nonlinear behavior using digital circuits [2]. DPD allows PAs to be operated at high efficiency modes without sacrificing linearity, which is nowadays almost one of the essential units in high power base stations. In the past decades, many digital predistortion techniques have been developed. Conventional DPDs [3]-[11] are mainly designed for single band transmitters and a couple of new approaches [12]-[30] have been proposed to deal with concurrent multi-band transmitters. Among them, 2D (two-dimensional)- DPD is the most popular one that originally proposed by S. A. Bassam et al. in [15]. 2D-DPD can compensate for the distortion in each band separately by treating the signal at two bands as two independent inputs. Most existing multi-band DPDs follow the similar idea. Liu et al. proposed a two-dimensional modified memory polynomial (2D-MMP) model [19] and a 2D augmented Hammerstein model [20] to reduce the complexity of the conventional 2D-DPD model while keeping the similar performance. L. Ding et al. [21] simplified the 2D-DPD model by proposing two efficient implementation schemes based on look-up tables. C. Quindroit et al. [22], [23] and Yang et al. [24] proposed an orthogonal 2D-DPD to improve the stability of the conventional model. M. Younes et al. [25] and M. Rawat et al. [26] employed the 2D-DPD model to compensate for hardware impairments. M. Younes et al. [27] extended 2D-DPD to a 3D-DPD for linearization of a concurrent tri-band PA and further developed a 3D phase-aligned pruned Volterra model [28]. Recently, M. Cabarkapa et al. [29] proposed a generalized 2D-DPD architecture based on simultaneous injection of in-band intermodulation and cross-modulation distortion products while B. Fehri et al. [30] proposed a dual-band baseband equivalent (BBE) Volterra model to reduce the complexity of conventional 2D-DPD model.

The 2D-DPD-based models have the advantages of reducing the sampling rate of analog to digital converters (ADCs) by only capturing the distortion surrounding the bands of interest. However, due to the inherent limitations of the model structure, multiple feedback loops are required to capture the output signals for each band simultaneously, which increases system implementation cost when the number of bands increases. Furthermore, separate models must be constructed for each band in the system. This implies that the complexity of this

This work was supported in part by the Science Foundation Ireland under the Investigator Award.

C. Yu and A. Zhu are with the School of Electrical, Electronic and Communications Engineering, University College Dublin, Dublin 4, Ireland (e-mail: chao.yu@ucdconnect.ie; anding.zhu@ucd.ie).

J. Xia and X. Zhu are with the State Key Laboratory of Millimeter Waves, Southeast University, Nanjing 210096, China (e-mail:jingxia@seu.edu.cn; xwzhu@seu.edu.cn).

system will greatly increase when the number of bands is greater than three.

In order to develop a low complexity and generalized DPD scheme for the multi-band transmitters, a single feedback loop-based DPD architecture was proposed in [31]. Unlike the 2D-DPD model, where multiple feedback loops are required to capture signals at the different frequency bands separately, only one single feedback observation path is required in this new structure. The proposed DPD approach also keeps the model structure the same as that in the conventional model for the single band transmitter, namely, the number of model coefficients in the proposed model is fixed, regardless of the number of the bands. Due to limited space, only basic model structure was given in [31]. In this paper, a thorough theoretical analysis and detailed model derivations are provided to give a complete description of the proposed approach. By employing the band-limited DPD approach in [32] and a carrier relocation technique in digital signal processing, the signal bandwidth of the DPD system can be further reduced, which provides more flexibilities to deal with ultra wideband scenarios in future concurrent multi-band transmitters. Extensive experimental tests have been conducted to validate various cases.

The rest of the paper is organized as follows. In Section II, the existing 2D-DPD based multi-band DPD architecture is briefly reviewed while the proposed multi-band DPD architecture is introduced in Section III. Experimental results are given in Section IV with a conclusion in Section V.

II. Existing Multi-band DPD

Different from the single band system, the signal in the concurrent multi-band system is transmitted simultaneously at multiple frequency bands and the frequency gaps among these bands are often very large. Due to the nonlinearities induced by the RF power amplifier, the frequency components of the output signal normally spread over a very wide range of frequency bands. It is almost impossible to capture all these distortion simultaneously because the bandwidth is too wide. In the mean time, it is often not necessary to linearize all the bands because only the distortion surrounding the main carriers are our concern and the rest of the distortion can be filtered by employing band-pass filters.

Considering this scenario, models based on the 2D-DPD structure [15] were proposed to linearize the concurrent multi-band transmitter. In this system, the signals at different bands are treated as independent inputs and fed into the model to linearize each band separately, as illustrated in Fig. 1. Since only distortion near each carrier is required to be captured, the sampling rates of ADCs at the feedback data observation path are significantly reduced. Because the input at each band is treated independently, the bandwidth of the signal to be processed in digital domain is also reduced. However, multiple DPD models must be employed because different nonlinear functions are used at each band, as expressed in (1).

$$\begin{cases} \tilde{u}_1(n) = F_1\left[\tilde{x}_1(n), \tilde{x}_2(n), ..., \tilde{x}_K(n)\right] \\ \tilde{u}_2(n) = F_2\left[\tilde{x}_1(n), \tilde{x}_2(n), ..., \tilde{x}_K(n)\right] \\ \quad \vdots \\ \tilde{u}_K(n) = F_K\left[\tilde{x}_1(n), \tilde{x}_2(n), ..., \tilde{x}_K(n)\right] \end{cases} \tag{1}$$

where $\tilde{x}_k(n)$ and $\tilde{u}_k(n)$ (k=1,2,…,K) are the baseband representation of the k^{th} band of input and output signal, respectively. $F_k(\cdot)$ is the transfer function at the k^{th} band. This leads that the number of coefficients employed in this system will exponentially increase with the number of bands involved. The authors in [28] have given an implication for this phenomenon and indicated that 315 (=105×3 bands) in total are required in a tri-band transmitter, even only for a nonlinearity order of 5 and a memory length of 3. Furthermore, the nonlinear terms in each model must be carefully selected in order to make sure the spectra of the signals generated from these terms will fall into the dedicated frequency bands. This process will become very difficult in the system where the number of bands is greater than three. Moreover, in this system, the nonlinear distortion spectra between the neighboring bands at the output of the PA must not overlap with each other, otherwise the DPD will not work properly.

Because each DPD output must be simultaneously generated from multiple independent inputs, $\tilde{x}_1(n)$, $\tilde{x}_2(n)$, … , $\tilde{x}_K(n)$, the outputs at different bands, $\tilde{y}_1(n)$, $\tilde{y}_2(n)$, …, $\tilde{y}_K(n)$, must be captured at the same time in order to extract and update the DPD coefficients. This causes that multiple feedback loops in the observation path must be employed and accurate synchronizations between all branches must be guaranteed in order to keep good linearization performance. A typical 2D-DPD system configuration is shown in Fig. 2.

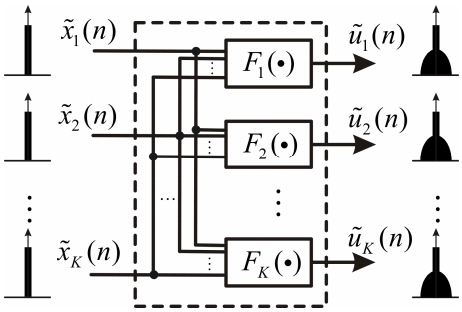

Fig.1. The existing multi-band DPD model.

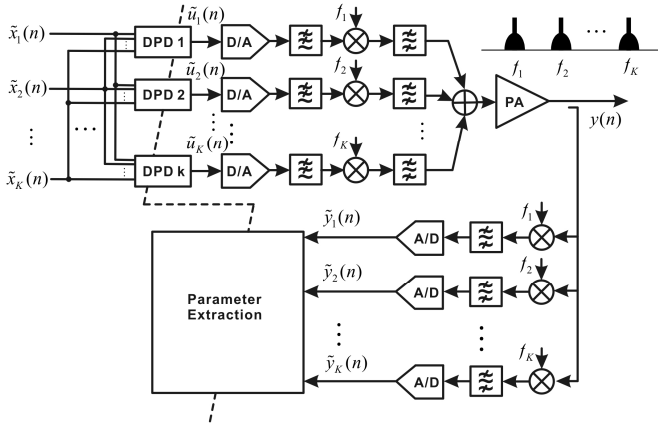

Fig.2. The existing multi-band DPD architecture.

III. Proposed Single-Model Single-Feedback DPD

The motivation behind the 2D-DPD was to reduce the bandwidth requirement of the system; however, it resulted that the DPD transfer functions for each band need to be built separately. In other words, all the DPD functions must be treated differently. This approach is very effective for dual- and tri-band systems, but the system complexity will dramatically increase if more than three bands are involved. This leads that we have to rethink about this approach and see if we could resolve this issue in a different way.

A. Carrier Relocation and Bandwidth Reduction

Let us re-look at the original system, we know that the PA behavior may change at the different bands, but the main property of the transfer function remains similar, especially in order to satisfy the data transmission requirement in carrier aggregation. The reason why we use different function for each band in 2D-DPD is because the input signal at each band is treated separately. If, however, we put all the input signals together as one composite input, we can simply use one common model to characterize the nonlinearity of the PA, that is

$$\begin{aligned} y(n) &= F_{PA}\left[\tilde{x}_1(n), \tilde{x}_2(n), ..., \tilde{x}_K(n)\right] \\ &= F_{PA}\left\{\tilde{x}_1(n)e^{j2\pi f_1 nT} + \tilde{x}_2(n)e^{j2\pi f_2 nT} + ... + \tilde{x}_K(n)e^{j2\pi f_K nT}\right\} \end{aligned} \quad (2)$$

where $y(n)$ is a composite multi-band signal of PA output and $F_{PA}(\cdot)$ represents the common transfer function. To separate the distortion at each band, a linear filter can be used, shown in Fig. 3a. The model can be expressed as,

$$y_k(n) = F_{PA}\left[\tilde{x}_1(n), \tilde{x}_2(n), ..., \tilde{x}_K(n)\right] * w_k(n), k = 1, 2, ..., K \quad (3)$$

where $*$ represents convolution operation, and w_k represents the filtering function for k^{th} band, and

$$y_k(n) = \tilde{y}_k(n)e^{j2\pi f_k nT}, k = 1, 2, ..., K \quad (4)$$

where $y_k(n)(k = 1,2, \dots, K)$ are the captured k^{th} band PA output located at f_k , and $\tilde{y}_k(n)(k = 1,2, \dots, K)$ are its corresponding baseband representation. This obviously returns to the original problem: the bandwidth of the signal is too wide, which is not feasible in digital implementation.

As mentioned earlier, in a concurrent multi-band system, although the composite signal bandwidth is wide, only limited distortion near each carrier band are our concern and the objective of the DPD is to generate the predistorted signals to compensate the distortion near each carrier only. From digital signal processing point of view, the frequency space in the carrier gap does not contain any useful information for DPD model construction. In other words, where the carrier frequency is allocated does not affect the predistortion signal generation. Therefore, the carrier frequencies, e.g., $f_1, f_2, \dots, f_K$, can be relocated nearby each other, e.g., $f_1', f_2', \dots, f_K'$, the input and output relationship of the PA can still be constructed, that is,

$$\begin{aligned} y'(n) &= F'_{PA}\left[\tilde{x}_1(n), \tilde{x}_2(n), ..., \tilde{x}_K(n)\right] \\ &= F'_{PA}\left\{\tilde{x}_1(n)e^{j2\pi f_1' nT} + \tilde{x}_2(n)e^{j2\pi f_2' nT} + ... + \tilde{x}_K(n)e^{j2\pi f_K' nT}\right\} \end{aligned} \quad (5)$$

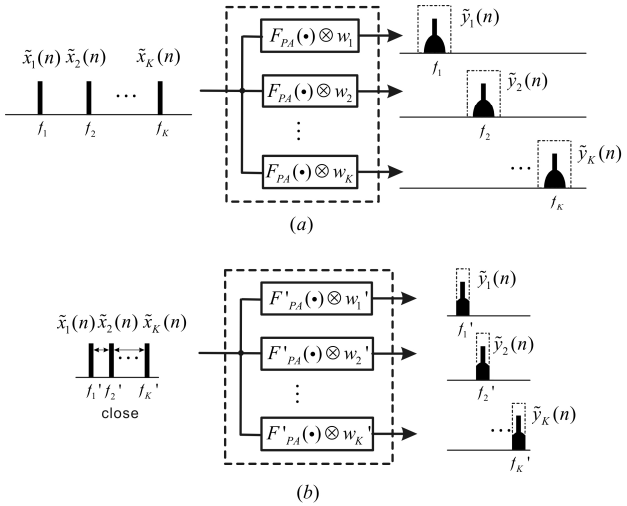

Fig. 3. Band-limited multi-band DPD scenario. (a) Original system. (b) New system with carrier relocation technique.

where $y'(n)$ is a new composite multi-band signal. $F'_{PA}(\cdot)$ represents the new common transfer function. In (5), the signal bandwidth can be reduced, but this is only workable when the frequency spectra of the signals between the bands do not overlap. This is difficult to satisfy because the distortion generated in the output of the PA often spread over all the places.

Recently, a band-limited Volterra series was proposed in [32], where a band-limiting function is inserted into the general Volterra operators to control the model bandwidth so that the bandwidth of the model output can exactly match that of the system under modeling. This approach not only increases PA model accuracy but also can be directly employed in DPD model construction, in particular, allowing users to choose the bandwidth to be linearized in the PA output according to the system requirement without sacrificing performance. In this paper, we extend this approach to the multi-band scenario and combine it with the carrier relocation technique to form a generalized single-model based multi-band DPD with reduced bandwidth, as described below.

To illustrate the idea, we take a tri-band scenario as an example. Let's assume the original carrier frequencies are at $f_1 = 2.1$ GHz, $f_2 = 2.4$ GHz, and $f_3 = 2.7$ GHz, and each band occupies 40 MHz bandwidth. If this signal passes a power amplifier with 7$^{\text{th}}$-order nonlinearity, the output at each band will occupy 280 MHz plus intermodulation products spreading over other bands. The total composite signal will occupy more than 840 MHz from 1.9 to 2.9 GHz at the PA output. This is very difficult to use a single DPD model to linearize this system. Even if we use the 2D-DPD approach, the bandwidth at each band is also very wide. Fortunately, in the real system, it is often not necessary to use DPD to compensate all the distortion. For instance, in this case, DPD may only be used to remove distortion near each carrier for 100 MHz. The rest of distortion can be attenuated by using a band-pass filter. This means that we only need to construct a model to map from three 40 MHz inputs to 100 MHz output and inverse it at each band. To do so, we can first limit the bandwidth of the model output at each band to 100 MHz by employing the band-limited approach and

then use the carrier relocation technique to move the signal close to each other, the model function can be expressed as

$$y_k'(n) = F'_{PA}\left[x_1(n), x_2(n), \ldots, x_K(n)\right] \cdot w_k'(n), k = 1, 2, \ldots, K \tag{6}$$

where $w_k'(\cdot)(k = 1,2, \ldots, K)$ is the band-limiting function for the k^{th} band after carrier relocation and

$$y_k'(n) = y_k(n)e^{j2\pi f_k' nT}, k = 1, 2, \ldots, K \tag{7}$$

where $y_k'(n)(k = 1,2, \ldots, K)$ are the captured k^{th} band PA output located at f_k' after carrier relocation. In this case, the total composite signal will only need to cover 300 MHz. The idea is illustrated in Fig. 3b and the detailed proof is given in Appendix.

B. Single-Model Predistorter

As demonstrated in [32], as long as the one to one mapping from input to output is correctly established, the DPD model can be constructed in the exact same way as that for the PA. Therefore, we can use the same approach to construct the multi-band DPD model.

Firstly, we let the baseband signals $\tilde{x}_1(n), \tilde{x}_2(n), \ldots, \tilde{x}_K(n)$ pass a carrier relocation module to form a composite multi-band signal based on the carrier relocation technique, for instance, it can be expressed as,

$$x'(n) = \sum_{k=1}^{K} x_k(n)e^{j2\pi f_k' nT} \tag{8}$$

where $x'(n)$ represents the new input signal after carrier relocation. Secondly, because a composite signal is used, a single common DPD transfer function $F'(\cdot)$ in the time domain can be constrctued to represent the inverse behavior of the PA and then the band-limiting functions can be used to redistrubute the predistorted signal to different bands. To facilitate expression, we combine the band-limitting functions together to form a new multi-band filtering function $w'(\cdot)$, that is

$$w'(n) = \sum_{k=1}^{K} w_k'(n) \tag{9}$$

The predistorted input signal $u'(n)$ can be represented by

$$\begin{aligned} u'(n) &= F'[x'(n)] \cdot w'(n) \\ &= F'\left[x_1(n), x_2(n), \ldots, x_K(n)\right] \cdot w'(n) \end{aligned} \tag{10}$$

and

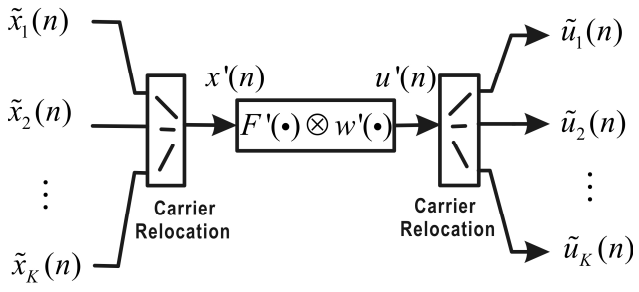

Fig.4. The proposed multi-band DPD model.

$$u'(n) = \sum_{k=1}^{K} u_k(n)e^{j2\pi f_k' nT} \tag{11}$$

where $\tilde{u}_k(n)(k = 1,2, \ldots, K)$ are the corresponding baseband representations of the k^{th} band DPD output located at f_k', that is,

$$\begin{cases} u_1(n) = \left(F'\left[x_1(n), x_2(n), \ldots, x_K(n)\right] \cdot w_1'(n)\right) e^{-j2\pi f_1' nT} \\ u_2(n) = \left(F'\left[x_1(n), x_2(n), \ldots, x_K(n)\right] \cdot w_2'(n)\right) e^{-j2\pi f_2' nT} \\ \quad \vdots \\ u_K(n) = \left(F'\left[x_1(n), x_2(n), \ldots, x_K(n)\right] \cdot w_K'(n)\right) e^{-j2\pi f_K' nT} \end{cases} \tag{12}$$

Finally, after obtaining the predistorted baseband signal for each band, the carrier frequency can be restored to the original value and the predistorted signal is redistributed to the required carrier frequency. This whole process is illustrated in Fig. 4.

Compared to the 2D-DPD model in Fig. 1, there are at least four distinctions in the proposed approach: (1) Only one DPD model is employed. (2) There is no need to select certain terms in the model in order to separate signals falling in different bands. The frequency selection process is done by applying a simple linear band-limiting function on the model. (3) Because a composite signal is used as input, the bandwidth of the signal to be processed by the model is of course wider than that at each band. But the bandwidth under linearization can be arbitrarily controlled by changing the bandwidth of the band-limiting function. The total signal processing bandwidth can be made comparable with that in 2D-DPD after applying the band-limiting approach. (4) Data synchronization during model extraction becomes much easier since the output data at different bands are not necessarily captured at the same time, which alleviates timing issue. This feature also results in a significant simplification of the DPD architecture, that is, a single feedback loop can be employed in model extraction, as discussed below.

C. Single-Feedback Model Extraction

In order to generate the DPD model, one of the key procedures is to extract the model coeffcients. Here, we use the band-limited Volterra serries [32] as an example to construct the DPD model shown in Fig. 4, which can be expressed as

$$\begin{aligned} u'(n) = \sum_{p=1}^{P} \sum_{i_1=0}^{M} \cdots \sum_{i_p=0}^{M} & h_{p,BL}(i_1, \cdots, i_p) \\ & \cdot \left(\prod_{j=1}^{p} x'(n - i_j)\right) \cdot w'(n) \end{aligned} \tag{13}$$

where $h_{p,BL}(i_1, \cdots, i_p)$ represents the pth-order band-limited Volterra kernel for DPD transfer function $F'(\cdot)$. To extract the model coefficients, one of the straightforward approaches is to use the pth-order inverse theory [33]. We can simply swap the input and output of the model using the captured data from the PA input and output, namely, replacing the input $x'(n)$ in (13) by the captured output $y'(n)$ and the output $u'(n)$ by the original PA input $x'(n)$, that is,

$$x'(n)=\sum_{p=1}^{P}\sum_{i_1=0}^{M}\cdots\sum_{i_p=0}^{M}h_{p,BL}(i_1,\cdots,i_p)\cdot\left(\prod_{j=1}^{p}y'(n-i_j)\right)w'(n) \tag{14}$$

This, however, results that the PA output from each band must be captured at the same time because $y'(n)$ must be the composite output including all the outputs from different bands, i.e.,

$$y'(n)=\sum_{k=1}^{K}y_k'(n)=\sum_{k=1}^{K}\tilde{y}_k(n)e^{j2\pi f_k' nT} \tag{15}$$

where $y_k'(n)(k=1,2,\ldots,K)$ is the captured k^{th} band output located at f_k', and $\tilde{y}_k(n)(k=1,2,\ldots,K)$ is the corresponding baseband representation, shown in Fig. 5. This leads that multiple feedback loops are required for model extraction, which is the same problem that occurs in the existing 2D-DPD system as shown in Fig. 2.

In order to resolve this issue, in this work we propose to extract the PA model $F'_{PA}(\cdot)$ first and then build the DPD model by using modeled PA output. Considering $x'(n)$ and $y'(n)$ is the input and the output of the PA, respectively, the PA model can be expressed as,

$$y'(n)=\sum_{p=1}^{P}\sum_{i_1=0}^{M}\cdots\sum_{i_p=0}^{M}h_{p,BL}^{PA}(i_1,\cdots,i_p)\cdot\left(\prod_{j=1}^{p}x'(n-i_j)\right)w'(n) \tag{16}$$

where $h_{p,BL}^{PA}(i_1,\cdots,i_p)$ represents the pth-order band-limited Volterra kernel for the new PA transfer function $F'_{PA}(\cdot)$.

The output at each band can be obtained by using the band-limiting function in (9),

$$\begin{aligned}
y_1'(n)&=\sum_{p=1}^{P}\sum_{i_1=0}^{M}\cdots\sum_{i_p=0}^{M}h_{p,BL}^{PA}(i_1,\cdots,i_p)\cdot\left(\prod_{j=1}^{p}x'(n-i_j)\right)w_1'(n)\\
y_2'(n)&=\sum_{p=1}^{P}\sum_{i_1=0}^{M}\cdots\sum_{i_p=0}^{M}h_{p,BL}^{PA}(i_1,\cdots,i_p)\cdot\left(\prod_{j=1}^{p}x'(n-i_j)\right)w_2'(n)\\
&\vdots\\
y_K'(n)&=\sum_{p=1}^{P}\sum_{i_1=0}^{M}\cdots\sum_{i_p=0}^{M}h_{p,BL}^{PA}(i_1,\cdots,i_p)\cdot\left(\prod_{j=1}^{p}x'(n-i_j)\right)w_K'(n)
\end{aligned} \tag{17}$$

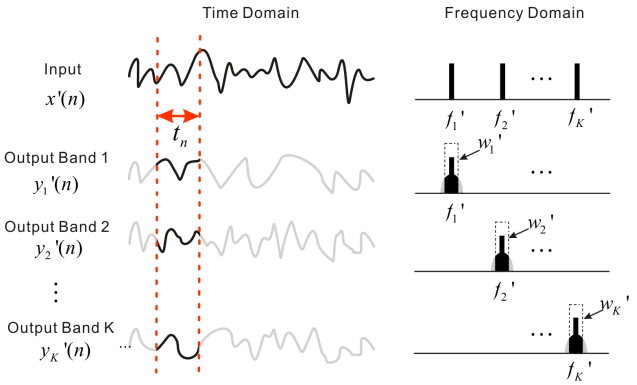

Fig.5. Signal synchronization process for the conventional model.

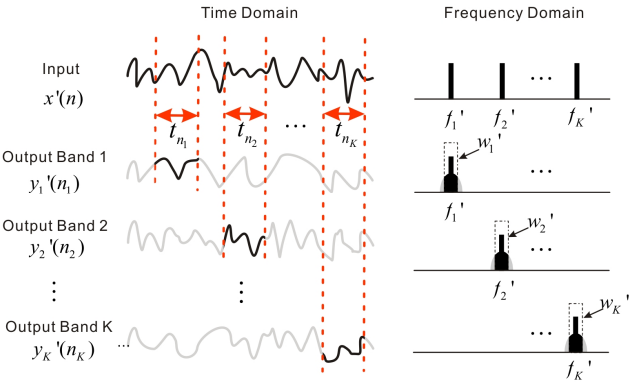

Fig.6. Signal synchronization process for the proposed model.

From (17), we can see that, in all the sub-functions, the same model $h_{p,BL}^{PA}(i_1,\cdots,i_p)$ and the same input signal $x'(n)$ are used. From modeling point of view, the time index n in each sub-function can be different. In other words, if replacing the simultaneous time index n with different ones n_1, $n_{2,\ldots,}$ n_K, the sub-functions become

$$\begin{aligned}
y_1'(n_1)&=\sum_{p=1}^{P}\sum_{i_1=0}^{M}\cdots\sum_{i_p=0}^{M}h_{p,BL}^{PA}(i_1,\cdots,i_p)\cdot\left(\prod_{j=1}^{p}x'(n_1-i_j)\right)w_1'(n_1)\\
y_2'(n_2)&=\sum_{p=1}^{P}\sum_{i_1=0}^{M}\cdots\sum_{i_p=0}^{M}h_{p,BL}^{PA}(i_1,\cdots,i_p)\cdot\left(\prod_{j=1}^{p}x'(n_2-i_j)\right)w_2'(n_2)\\
&\vdots\\
y_K'(n_K)&=\sum_{p=1}^{P}\sum_{i_1=0}^{M}\cdots\sum_{i_p=0}^{M}h_{p,BL}^{PA}(i_1,\cdots,i_p)\cdot\left(\prod_{j=1}^{p}x'(n_K-i_j)\right)w_K'(n_K)
\end{aligned} \tag{18}$$

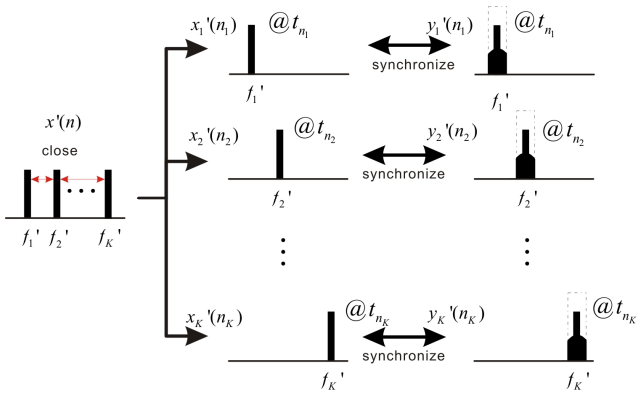

Fig. 7.The details for signal synchronization process.

But the model stays the same. The only difference is that the output at different band is synchronized to different time segment of the composite signal, as illustrated in Fig. 6. This character results in a very important advantage: in the PA model extraction, we can use a single feedback loop to capture the output at different bands and at different time seperately. We then can synchronize with the same reference signal $x'(n)$, similar to selective sampling [34]. The synchronization process is illustrated in Fig. 7. This allows different bands to share the same feedback loop and thus the number of feedback loops can be reduced to only one, no matter how many transmit bands are involved, which significantly reduces the structure complexity. Furthermore, because the linearized bandwidth is selected by the band-limiting function in the proposed model, there is no need to capture the full bandwidth information at each band. Only a single narrow band feedback loop is required to be employed in the proposed architecture. For instance, in the tri-band example discussed earlier, only a single 100 MHz feedback loop is needed in the new system while three 280 MHz feedback loops are required if the 2D-DPD system is employed. Of course, un-linearized distortion must be filtered by analog filters in the transmitter chain. To switch between different bands, proper switching circuits must be deployed.

After data acquisition and synchronization, the next step is PA model extraction. In matrix form, all the equations in (18) can be represented by

$$\mathbf{Y}_{N'1}^{(k)} = \mathbf{X}_{N'L}^{(k)} \mathbf{C}_{L'1}, k = 1, 2, ..., K \tag{19}$$

where N is the number of data samples and L is the number of coefficients. $\mathbf{C}$ is the coefficients matrix,

$$\mathbf{C}_{L'1} = \begin{bmatrix} h_{1,BL}^{PA}(0,\mathbf{L},0) \\ \mathbf{M} \\ h_{3,BL}^{PA}(1,\mathbf{L},0) \\ \mathbf{M} \\ h_{P,BL}^{PA}(M,\mathbf{L},M) \end{bmatrix} \tag{20}$$

$\mathbf{Y}$ is the output matrix generated from the captured output after carrier relocation, that is, $y_k'(n_k)$ $(k = 1,2,...,K)$,

$$\mathbf{Y}_{N'1}^{(k)} = \begin{bmatrix} y_k'(n_k) \\ y_k'(n_k+1) \\ y_k'(n_k+2) \\ \mathbf{M} \\ y_k'(n_k+N-1) \end{bmatrix}, k = 1,2,...,K \tag{21}$$

$\mathbf{X}$ is the input matrix generated from the input $x'(n_k)$ $(k = 1,2,...,K)$, containing all linear and nonlinear model terms processed by the band-limiting functions $w_k'(\cdot)(k = 1,2,...,K)$, which is shown in (22) in the bottom of this page.

Because the model is shared among all the bands, the matrix assembled at each band are combined together, that is,

$$\begin{bmatrix} \mathbf{Y}_{N'1}^{(1)} \\ \mathbf{Y}_{N'1}^{(2)} \\ \mathbf{M} \\ \mathbf{Y}_{N'1}^{(K)} \end{bmatrix} = \begin{bmatrix} \mathbf{X}_{N'L}^{(1)} \\ \mathbf{X}_{N'L}^{(2)} \\ \mathbf{M} \\ \mathbf{X}_{N'L}^{(K)} \end{bmatrix} \mathbf{C}_{L'1} \tag{23}$$

The PA characteristics can then be extracted by employing the standard least squares (LS) algorithm since the model is linear-in-parameters. Thus,

$$\hat{\mathbf{C}}_{L'1} = \left(\begin{bmatrix} \mathbf{X}_{N'L}^{(1)} \\ \mathbf{X}_{N'L}^{(2)} \\ \mathbf{M} \\ \mathbf{X}_{N'L}^{(K)} \end{bmatrix}^H \begin{bmatrix} \mathbf{X}_{N'L}^{(1)} \\ \mathbf{X}_{N'L}^{(2)} \\ \mathbf{M} \\ \mathbf{X}_{N'L}^{(K)} \end{bmatrix} \right)^{-1} \begin{bmatrix} \mathbf{X}_{N'L}^{(1)} \\ \mathbf{X}_{N'L}^{(2)} \\ \mathbf{M} \\ \mathbf{X}_{N'L}^{(K)} \end{bmatrix}^H \begin{bmatrix} \mathbf{Y}_{N'1}^{(1)} \\ \mathbf{Y}_{N'1}^{(2)} \\ \mathbf{M} \\ \mathbf{Y}_{N'1}^{(K)} \end{bmatrix} \tag{24}$$

where $\hat{\mathbf{C}}$ is the extracted PA coefficient vector.

Once the coefficients of the PA model have been extracted,

$$\mathbf{X}_{N'L}^{(k)} = \begin{bmatrix} \sum_{s=0}^{S} x'(n_k - s) w_k'(s) & \mathbf{L} & \sum_{s=0}^{S} x'(n_k - 1 - s)\left(x'(n_k - s)\right)^2 w_k'(s) & \mathbf{L} & \sum_{s=0}^{S} \left(x'(n_k - M - s)\right)^P w_k'(s) \\ \sum_{s=0}^{S} x'(n_k + 1 - s) w_k'(s) & \mathbf{L} & \sum_{s=0}^{S} x'(n_k - s)\left(x'(n_k + 1 - s)\right)^2 w_k'(s) & \mathbf{L} & \sum_{s=0}^{S} \left(x'(n_k + 1 - M - s)\right)^P w_k'(s) \\ \sum_{s=0}^{S} x'(n_k + 2 - s) w_k'(s) & \mathbf{L} & \sum_{s=0}^{S} x'(n_k + 1 - s)\left(x'(n_k + 2 - s)\right)^2 w_k'(s) & \mathbf{L} & \sum_{s=0}^{S} \left(x'(n_k + 2 - M - s)\right)^P w_k'(s) \\ \mathbf{M} & \mathbf{M} & \mathbf{M} & \mathbf{M} & \mathbf{M} \\ \sum_{s=0}^{S} x'(n_k + N - 1 - s) w_k'(s) & \mathbf{L} & \sum_{s=0}^{S} x'(n_k + N - 2 - s)\left(x'(n_k + N - 1 - s)\right)^2 w_k'(s) & \mathbf{L} & \sum_{s=0}^{S} \left(x'(n_k + N - 1 - M - s)\right)^P w_k'(s) \end{bmatrix} \tag{22}$$

$(k = 1,2,...,K)$

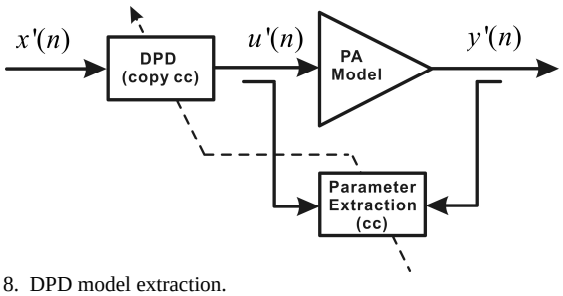

Fig. 8. DPD model extraction.

the synchronized composite output can be generated by using

$$\hat{\mathbf{Y}}_{N'1} = \mathbf{X}_{N'L}\hat{\mathbf{C}}_{L'1} \tag{25}$$

We now can have a composite input $x'(n)$ and a composite output $y'(n)$. Then we can return to (14) to extract the DPD model using the standard indirect learning technique [35]-[36] where the input $x'(n)$ and the reconstructed output $y'(n)$ are swapped, as shown in Fig. 8 and the LS algorithm can be employed again. This is a standard indirect learning process as described in most DPD literature. Only difference is that the PA output is generated from a pre-extracted model rather than the measurement. To avoid duplication, we omit further description.

D. The Complete DPD System

Based on the above descriptions, the complete multi-band DPD architecture can be constructed as shown in Fig. 9. In the transmitter chain, the baseband inputs $\tilde{x}_1(n),\ \tilde{x}_2(n), \ldots, \tilde{x}_K(n)$ at each band first pass through the Carrier Relocation module to construct a new composite multi-band input signal $x'(n)$ with reduced signal processing bandwidth. The predistorted input signal $u'(n)$ is then generated by using the proposed multi-band DPD model and re-distributed to multiple bands at output $\tilde{u}_1(n), \tilde{u}_2(n), \ldots, \tilde{u}_k(n)$ by using the second Carrier Relocation module. All the predistorted input signals are then combined together to be modulated and up-converted to the RF frequency to generate the real-valued predistorted input signal $u(n)$, which will be fed into the PA to obtain the linearized PA output $y(n)$. In the feedback loop, the output signal $\tilde{y}_1(n_1), \tilde{y}_2(n_2), \ldots, \tilde{y}_K(n_K)$ at each band is captured at different carrier frequency and at different time by using a shared single feedback loop and then synchronized with the input signal $u'(n)$. The synchronized outputs are used together with the original composite input signal $u'(n)$ first in the PA Modeling block to extract the PA model and then the indirect learning is used in the Parameter Extraction module to obtain DPD coefficients (*cc*). Finally, the coefficients (*cc*) are copied to the DPD Module.

IV. Experimental Results

To validate the proposed approach, we set up a wideband DPD platform as shown in Fig. 10. Multiple modulated multi-band signal sources are generated from MATLAB running on a PC and downloaded to a FPGA baseband board that is connected to an RF board. The signals at different bands are combined together in the baseband, up-converted to the RF frequency and fed into a single wideband PA that emulates a multi-band transmitter. The center frequency is operated at 2.55 GHz, and the P1dB compression point of the PA is at 46.4 dBm. In the feedback loop, the output of the PA is down-converted and captured at different time slots for each band with a sampling rate at 400 MSPS. Four sets of tests were conducted:(1) comparison between the proposed approach and the state-of-the-art 2D-DPD; (2) performance with various bands configuration;(3) dual-band signals with various carrier relocations to evaluate consistence of the model with bandwidth changes; (4) wideband dual-band signals to evaluate the capability of the proposed approach for handling band-limited conditions. The linearization performances in

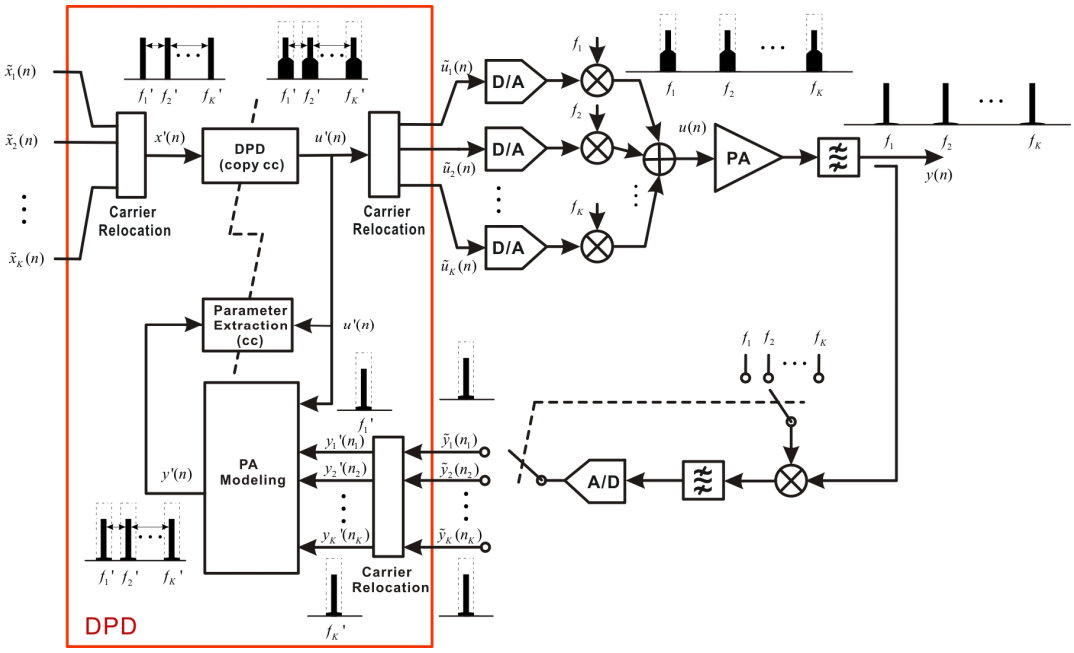

Fig. 9.The complete system architecture of the proposed DPD.

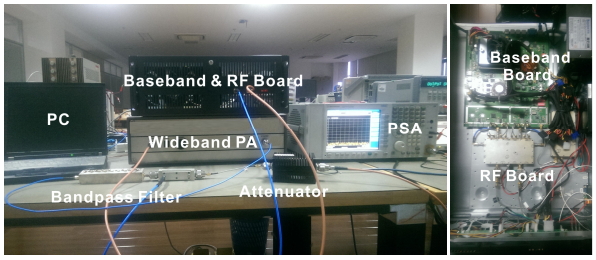

(a) (b)

Fig. 10. Test bench: (a) System setup; (b) Baseband & RF board

these tests are evaluated by adjacent channel power ratio (ACPR) in frequency domain and normalized root mean square error (NRMSE) in time domain.

A. *Proposed Approach vs 2D-DPD*

To compare with the state-of-the-art, we implemented the 2D-DPD technique published in [15] on our test bench. The exactly same system configuration was applied for both the model in [15] and the proposed approach except that, in 2D-DPD, the outputs at two bands were captured by using a repeated sequence twice to emulate the simultaneous data acquisition, while in the proposed approach, the outputs are captured at different time slots from one data sequence. In other words, in 2D-DPD the output data at two bands are synchronized with the same segment of the original input, as shown in Fig. 5, while in the proposed approach, the outputs are synchronized with different segments of the original input, as shown in Fig. 6. The dual-band signal is 20 MHz signals centered at 2.4 GHz and 2.7 GHz with power-to-average power ratio (PAPR) of 9 dB. The bandwidth of shared feedback loop is set as 100 MHz, and the frequency spacing (Δf) is 110 MHz.

In the 2D-DPD, the nonlinear order was set to 7 and the memory length was 3. The DPD function in the proposed model is the band-limited dynamic deviation reduction (DDR)-based Volterra model [32] with the decomposed piecewise technique [37]. The parameter for the model is set as the magnitude threshold of 0.5 for the normalized data, the nonlinearity order of {7,7}, and the memory length of {3, 3}. The band-limiting function is set according to the bandwidth requirement of the feedback loop. The performance comparison is shown in Fig. 11, where we can see that, although dual-band signals are captured at different time in proposed method, it can still achieve similar performance as that with the conventional 2D-DPD. The performance details are listed in the Table I. It is worth mentioning that the number of the coefficients of the 2D-DPD is 224 while the proposed approach only requires 86 coefficients.

TABLE I

THE MEASURED LINEARIZATION PERFORMANCE COMPARISONS BETWEEN 2D-DPD AND PROPOSED DPD

	ACPR(± 20 MHz) (dBc)		NRMSE (%)		No. of Coeff. (N=7,M=3)
	2400 MHz	2700 MHz	2400 MHz	2700 MHz	N/A
Without DPD	-37.9/ -36.5	-40.4/ -41.7	6.9	5.5	N/A
2D-DPD	-55.6/ -55.4	-55.4/ -54.2	1.1	1.6	224= 112*2 sets
Proposed DPD	-55.3/ -55.4	-55.5/ -55.6	1.1	1.7	86= 86*1 set

B. *Multi-band Signal Tests*

In this test, we validate the model with different band configurations. First, we tested evenly-spaced tri-band and quad-band scenarios: (1) a tri-band signal with evenly-spaced carriers at 2400 MHz, 2550 MHz, 2700 MHz (PAPR = 9.5 dB); (2) a quad-band signal with four carriers at 2400 MHz, 2500 MHz, 2600 MHz, 2700 MHz (PAPR = 9.0 dB). The signal at each band occupies 20 MHz. The same feedback loop is shared to capture all the distortion around the transmitted bands in the output. The DPD function in the proposed model is the same as that in Part A. The bandwidth of shared feedback loop is set as 80 MHz and 60 MHz, and the frequency spacing (Δf) of carrier relocation is set as {75, 75}, {60, 60, 60} for tri-band and quad-band cases, respectively. Fig. 12 shows the spectra plots and Table II gives the measured ACPR and NRMSE performance where we can see that excellent linearization performance can be achieved in all scenarios.

We then tested unevenly-spaced tri-band and quad-band scenarios. The system configurations were the same as those for evenly-spaced tri-band cases except different frequency spacing. As discussed in Appendix, in the unevenly-spaced case, part of intermodulation products between bands fall in the spaces between main carriers. To avoid frequency overlaps, the same frequency spacing ratio must be kept when conducting carrier relocation. In Case A, the frequency spacing is set as {60, 120}, which is proportional to the ratio of the actual RF frequency spacing. The test results are shown in Fig. 13 and Table II, where we can see that the distortion can be effectively compensated. Also as mentioned in Appendix, keeping the

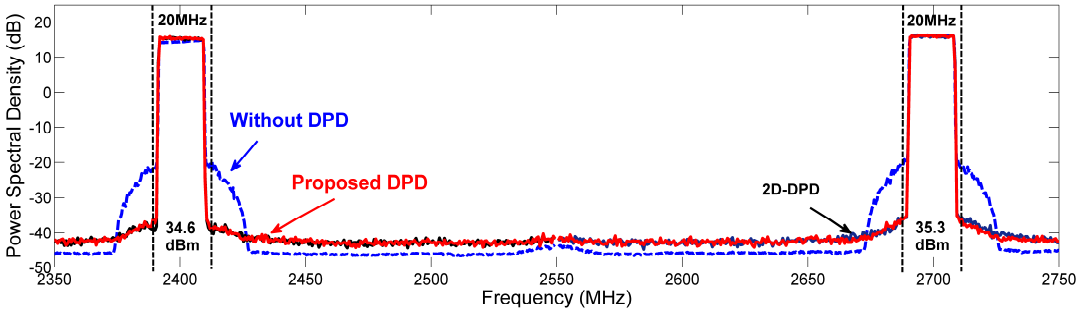

Fig.11. Measured power spectral density for 2D-DPD and the proposed DPD.

frequency spacing ratio may limit the bandwidth reduction in carrier relocation if the carriers are disproportionately spaced. To further reduce signal processing bandwidth in model extraction, we may need to allow some frequency overlaps. To test the performance, in Case B, we set the frequency spacing as {75, 75} for carrier relocation. This leads that the intermodulation products between Band 1 and Band 2 fall in Band 3 during DPD model extraction. The results are given in Fig. 13 and Table II, where we can see that the performance is slightly worse than that of Case A, but the degradation is relatively small. This leads a conclusion that in a real application, we can make a tradeoff between the performance and bandwidth requirement.

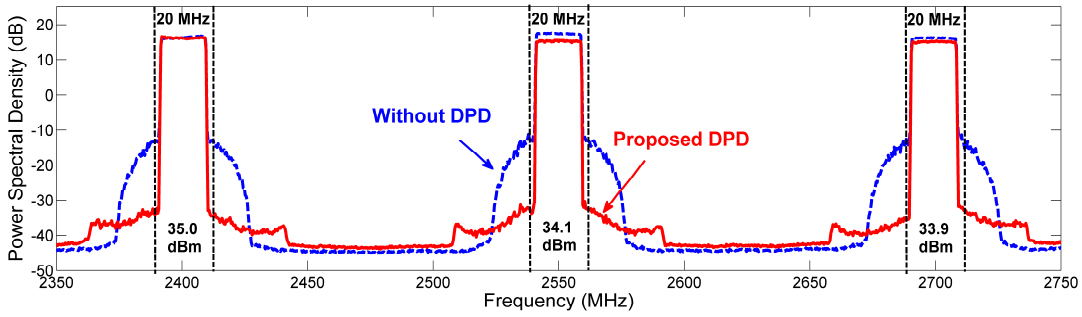

(a)

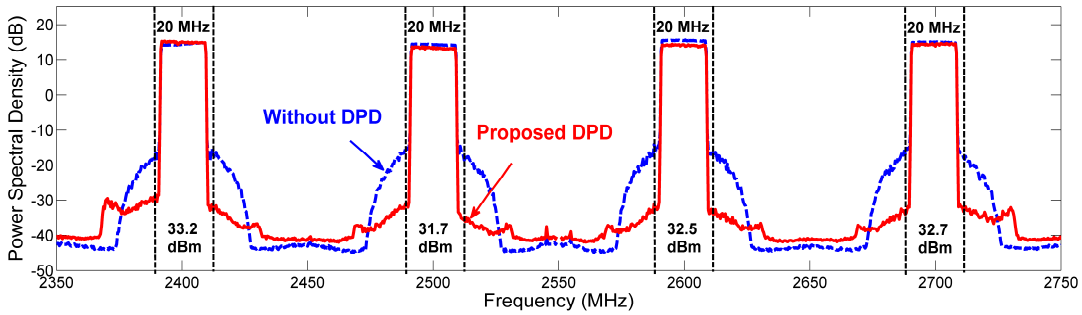

(b)

Fig.12. Measured power spectral density for evenly-spaced cases: (a) Tri-band (d) Quad-band.

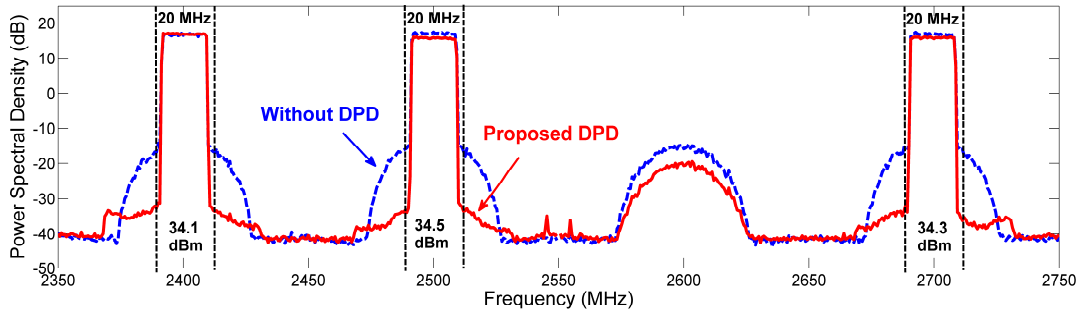

(a)

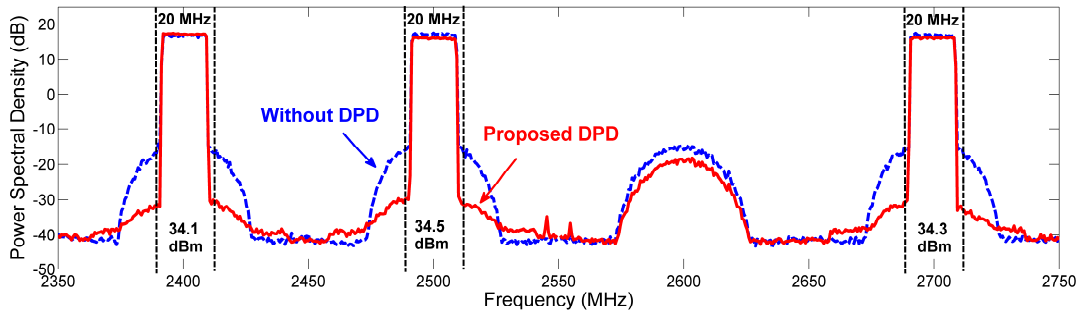

(b)

Fig.13. Measured power spectral density for unevenly-spaced cases: (a) Tri-band Case A (b) Tri-band Case B.

TABLE II

THE MEASURED LINEARIZATION PERFORMANCE COMPARISONS WITH/WITHOUT DPD UNDER DIFFERENT BAND CONFIGURATIONS

		ACPR(± 20 MHz) (dBc)			NRMSE (%)		
Scenario 1: Tri-band (even)		2400 MHz	2550 MHz	2700 MHz	2400 MHz	2550 MHz	2700 MHz
	Without DPD	-34.2/-33.1	-38.0/-38.5	-35.5/-36.4	6.8	6.2	6.5
	With DPD	-50.8/-51.7	-49.6/-49.8	-51.9/-49.5	1.5	1.8	2.5

Scenario 2: Quad-band (even)		2400 MHz	2500 MHz	2600 MHz	2700 MHz	2400 MHz	2500 MHz	2600 MHz	2700 MHz
	Without DPD	-36.7/-34.8	-37.9/-37.8	-38.9/-39.8	-37.4/-39.3	7.8	5.6	4.7	5.2
	With DPD	-46.9/-50.4	-50.1/-50.5	-50.4/-50.5	-50.2/-48.9	2.3	2.1	1.5	1.8

		2400 MHz	2500 MHz	2700 MHz	2400 MHz	2500 MHz	2700 MHz
Scenario 3: Tri-band (uneven)	Without DPD	-37.7/-36.5	-36.8/-37.0	-36.4/-37.7	4.20	4.36	4.21
	With DPD(Case A)	-51.0/-52.1	-52.1/-51.3	-51.1/-52.4	1.62	1.63	0.65
	With DPD(Case B)	-51.6/-50.3	-48.4/-49.1	-49.3/-51.4	1.61	1.65	0.83

C. Dual-band Tests with Various Carrier Relocations

In this section, we study how the frequency spacing (Δf) of the carrier relocation affects the linearization performance. In this test, all the settings for the proposed model are the same with those in Part A except the frequency spacing. The frequency spacing of carrier relocation is changed from 120 MHz to 160 MHz, with step of 10 MHz. The ACPRs and NRMSEs against the frequency spacing are plotted at Figs. 14-15. For the linearization performance for the lower band as shown in Fig. 14a, all the values of ACPRs (±20MHz) can reach around -54 dB, with only small fluctuations. Similar linearization performance for the upper band can be achieved as shown in Fig. 14b. From Fig. 15, the similar trends for NRMSEs can be found. The details for the linearization performance against different frequency spacing are listed in TABLE III. From the test results, we can conclude that frequency spacing does not affect the DPD linearization performance in the concurrent dual-band scenario.

D. Dual-band Tests with Limited Bandwidth

In this part, we further evaluate the capability of the proposed DPD model for dealing with limited (or incomplete) bandwidth information in a single narrowband feedback loop, which probably will occur in the future wideband concurrent multi-band systems. In this test, two wideband signals with bandwidth of 40 MHz are aggregated together to form a dual-band signal spanned in the 400 MHz bandwidth range. Due to the nonlinear spectrum regrowth in the frequency domain, the output bandwidth will spread over a wide bandwidth and it is very difficult to capture all the distortion. Here, we assume only 80 MHz bandwidth signal can be processed with 100 MHz frequency spacing of carrier relocation. Because it is very difficult to design a whole transceiver with variable bandwidths, the bandwidth for the

TABLE III

THE PERFORMANCE COMPARISONS UNDER DIFFERENT CARRIER RELOCATIONS

	ACPR(± 20 MHz)(dBc)		NRMSE (%)	
	2400 MHz	2700 MHz	2400 MHz	2700 MHz
Without DPD	-37.9/-36.5	-40.4/-41.7	6.9	5.5
Proposed Δf=120	-54.3/-54.4	-53.7/-54.8	0.98	1.3
Proposed Δf=130	-54.4/-54.2	-53.2/-54.2	0.95	1.4
Proposed Δf=140	-54.5/-54.1	-53.8/-55.4	1.0	1.4
Proposed Δf=150	-54.6/-53.6	-53.4/-54.6	0.98	1.4
Proposed Δf=160	-54.6/-54.1	-53.4/-54.9	0.98	1.3

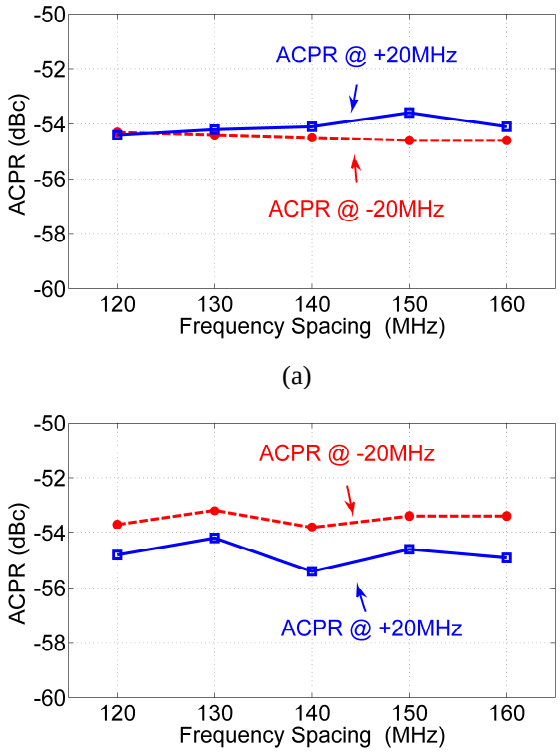

Fig. 14. Measured ACPR values under different carrier relocations. (a) lower band (b) upper band

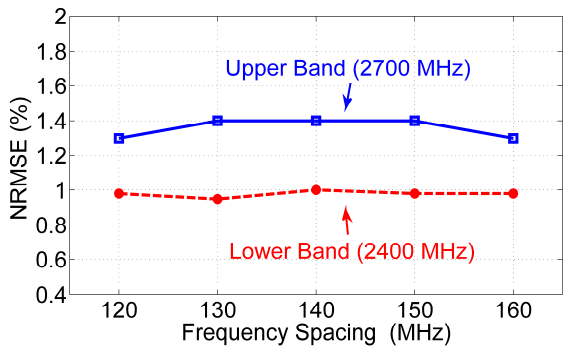

Fig. 15. Measured NRMSE values under different carrier relocations.

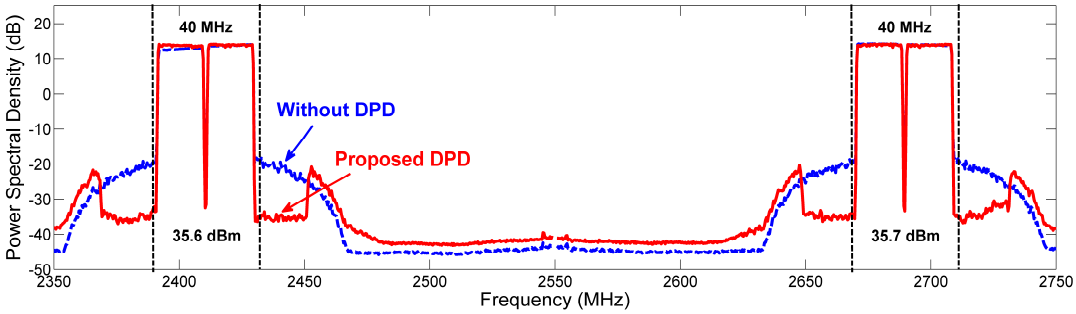

Fig. 16. Measured power spectral density under band-limited scenario.

TABLE IV
THE DPD PERFORMANCE COMPARISONS UNDER BAND-LIMITED SCENARIO

	ACPR(± 20 MHz)(dBc)		NRMSE (%)	
	2410 MHz	2690 MHz	2410 MHz	2690 MHz
Without DPD	-37.7/-38.7	-37.6/-38.1	6.7	4.4
With DPD	-51.3/-51.5	-51.2/-50.3	1.26	1.8

transmitter chain and observation path is fixed in our test. We limited the bandwidth of the predistorted input before sending it to PA and employed a fixed observation chain to capture the signals from the PA output, and then processed them in the digital domain to emulate the filtering effects of the PA output. Fig. 16 shows the measured power spectral density for the lower band and the upper band, where we can find that although the bandwidth of the feedback loop is limited, excellent linearization performance can still be achieved within the selected bandwidth, reaching -51 dBc for each carrier of the 40 MHz signal. The values of ACPR and NRMSE are listed in TABLE IV, which give a confirmation that the proposed model has the advantage of handling the scenario with limited bandwidth of feedback loop.

V. CONCLUSION

In this paper, a novel single-model digital predistortion technique has been proposed to linearize the concurrent multi-band transmitters by sharing a single narrowband feedback loop for data acquisition. Compared to the existing 2D-DPD models, the proposed approach provides a much enhanced flexibility for dealing with wideband concurrent multi-band operations, in particular with reduced model complexity and a simpler system structure. As demonstrated in the experimental tests, the proposed approach is scalable with bandwidth at each band and its performance is consistent under various band configurations. It provides a promising solution for reducing implementation complexity and cost for future multi-band DPD systems.

APPENDIX
DERIVATION OF CARRIER RELOCATION TECHNIQUE WITH BANDWIDTH REDUCTION

In this appendix, the detailed proof for the proposed carrier relocation technique is provided. We first define the composite multi-band input $x(n)$ and output $y(n)$ of the PA as

$$x(n) = \sum_{k=1}^{K} \tilde{x}_k(n) e^{j2\pi f_k nT} \tag{A.1}$$

$$y(n) = \sum_{k=1}^{K} \tilde{y}_k(n) e^{j2\pi f_k nT} \tag{A.2}$$

where $\tilde{x}_k(n)$, $\tilde{y}_k(n)(k = 1,2,\ldots,K)$ are the corresponding baseband representations of the k^{th} band of PA input and output located at the carrier frequency f_k. To simplify derivation, we use a memoryless system with nonlinearity order of P to represent the PA as an example, expressed in (A.3),

$$y(n) = \sum_{p=0}^{(P-1)/2} a_{2p+1} \left|x(n)\right|^{2p} x(n) \tag{A.3}$$

where P is an odd number and only the odd-order terms are considered. By employing the band-limited modeling technique [32], a multiband band-limiting function $w(\cdot)$ can be introduced into (A.3),

$$y(n) = \sum_{p=0}^{(P-1)/2} a_{2p+1} \left(\left(\left|x(n)\right|^{2p} x(n) \right) \ddot{A}\, w(n) \right) \tag{A.4}$$

where $\ddot{A}$ represents convolution operation, and

$$w(n) = \sum_{k=1}^{K} w_k(n) \tag{A.5}$$

where $w_k(\cdot)(k = 1,2,\ldots,K)$ is the band-limiting function for the k^{th} band. To represent the carrier frequency information $e^{j2\pi f_k nT}$, we define $w_{k,0}$ as the low-pass equivalent representation of the band-pass filter $w_k(\cdot)$ at center frequency f_k, that is

$$w_k(n) = w_{k,0}(n) e^{j2\pi f_k nT}, k = 1,2,\ldots,K \tag{A.6}$$

Substituting (A.1) and (A.5) into (A.4), the output $y(n)$ can be obtained,

$$y(n) = \sum_{p=0}^{(P-1)/2} a_{2p+1} \left| \sum_{k=1}^{K} \tilde{x}_k(n) e^{j2\pi f_k nT} \right|^{2p} \sum_{k=1}^{K} \tilde{x}_k(n) e^{j2\pi f_k nT} \ddot{A} \left(\sum_{k=1}^{K} w_k(n) \right) \tag{A.7}$$

Expanding (A.7), we can obtain

$$y(n)=\sum_{p=0}^{(P-1)/2} a_{2p+1}\left(\sum_{k=1}^{K} x_k(n)e^{j2\pi f_k nT}\right)^{p+1}\left(\sum_{k=1}^{K} x_k^*(n)e^{-j2\pi f_k nT}\right)^{p}\left(\sum_{k=1}^{K} w_k(n)\right)$$

$$=\sum_{p=0}^{(P-1)/2} a_{2p+1}\left(\sum_{i_1=1}^{K}\sum_{i_2=1}^{K}\cdots\sum_{i_{2p+1}=1}^{K}\prod_{j=1}^{p+1} x_{i_j}(n)\prod_{j=p+2}^{2p+1} x_{i_j}^*(n)e^{j2\pi\left(\sum_{j=1}^{p+1} f_{i_j}-\sum_{j=p+2}^{2p+1} f_{i_j}\right)nT}\right)\left(\sum_{k=1}^{K} w_k(n)\right) \tag{A.8}$$

From (A.8), we can find that the frequency components of the output are centered at different carrier frequencies that can be represented by

$$f=\sum_{j=1}^{p+1} f_{i_j}-\sum_{j=p+2}^{2p+1} f_{i_j}, \tag{A.9}$$

as shown in Fig. A-1 for a tri-band scenario. We can see that the frequency spaces between each frequency component are empty and thus no information is carried in these spaces. From the behavioral modeling point of view, these spaces do not contribute any value to the model construction which maps input to output of the PA. To reduce the signal processing bandwidth, the frequency components at the PA output can be relocated closer to each other without losing any information. We call this technique, *carrier relocation*.

In multiband operation, carrier frequencies are usually located in two scenarios: *evenly-spaced* and *unevenly-spaced*. In the evenly-spaced case, the near band distortion generated from each band fall on main carriers and thus these are no intermodulation products located between the main carriers. During the model extraction, the carrier frequencies can then be *relocated* closely to each other, as shown in Fig. A-1a. However, in the unevenly-spaced case, there are some intermodulation products located between the main carriers. For instance, as shown in Fig. A-1b, the intermodulation products of f_1 and f_2 are located between f_2 and f_3. In this case, we have to avoid frequency overlaps when we conduct the carrier relocation. This can be achieved by keeping the ratio of

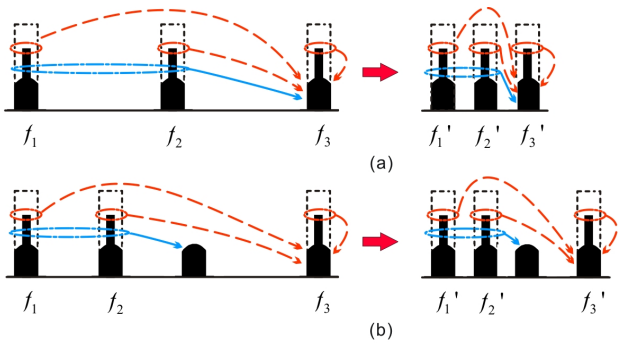

Fig. A-1. Carrier relocation: (a) evenly-spaced; (b) unevenly-spaced

the relocated carrier frequencies the same as that of the original frequencies.

To illustrate how this works, let's take the distortion at band 3 in the tri-band scenario shown in Fig. A-1b as an example. Firstly, grouping all the terms located at f_3 generated by different frequency combinations, that is

$$f_3=\sum_{j=1}^{p+1} f_{i_j}-\sum_{j=p+2}^{2p+1} f_{i_j} \tag{A.10}$$

(A.8) can be reformulated as

$$y_3(n)=\sum_{p=0}^{(P-1)/2} a_{2p+1}\left(\sum_{i_1=1}^{K}\sum_{i_2=1}^{K}\cdots\sum_{i_{2p+1}=1}^{K}\prod_{j=1}^{p+1} x_{i_j}(n)\prod_{j=p+2}^{2p+1} x_{i_j}^*(n)e^{j2\pi f_3 nT}\right)w_3(n) \tag{A.11}$$

Substituting (A.6) into (A.11) and combining the convolution operation, we can obtain

$$y_3(n)=\sum_{p=0}^{(P-1)/2} a_{2p+1}\left(\sum_{i_1=1}^{K}\sum_{i_2=1}^{K}\cdots\sum_{i_{2p+1}=1}^{K}\prod_{j=1}^{p+1} x_{i_j}(n)\prod_{j=p+2}^{2p+1} x_{i_j}^*(n)\right)*w_{3,0}(n)\,e^{j2\pi f_3 nT} \tag{A.12}$$

where $y_3(n)$ represents the frequency component located at frequency f_3 in the output.

Now, in order to do carrier relocation, the relationship between carrier frequencies can be represented by

$$\frac{f_k-f_1}{f_2-f_1}=\frac{f_k'-f_1'}{f_2'-f_1'}\,(k=1,2,\ldots,K) \tag{A.13}$$

where $f_k'(k=1,2,\ldots,K)$ is the relocated carrier frequency.

Combining (A.10) and (A.13), the new relocated frequency is

$$f_3'=\sum_{j=1}^{p+1} f_{i_j}'-\sum_{j=p+2}^{2p+1} f_{i_j}' \tag{A.14}$$

Then, following the same procedure, the distortion located at band 3 can be represented by the relocated frequencies, that is,

$$y_3'(n)=\sum_{p=0}^{(P-1)/2} a_{2p+1}\left(\sum_{i_1=1}^{K}\sum_{i_2=1}^{K}\cdots\sum_{i_{2p+1}=1}^{K}\prod_{j=1}^{p+1} x_{i_j}(n)\prod_{j=p+2}^{2p+1} x_{i_j}^*(n)\right)*w_{3,0}(n)\,e^{j2\pi f_3' nT} \tag{A.15}$$

where $y_3'(n)$ represents the frequency component located at frequency f_3' in the output.

Finally, comparing (A.12) and (A.15), we can find that the baseband information is the same at these carrier frequencies,

$$y_3'(n)=\sum_{p=0}^{(P-1)/2} a_{2p+1}\left(\sum_{i_1=1}^{K}\sum_{i_2=1}^{K}\cdots\sum_{i_{2p+1}=1}^{K}\prod_{j=1}^{p+1} x_{i_j}(n)\prod_{j=p+2}^{2p+1} x_{i_j}^*(n)\right)*w_{3,0}(n) \tag{A.16}$$

From the derivations above, we can conclude that as long as the frequency spacing ratio is kept the same, the baseband information of the output $\tilde{y}_k(n)\,(k=1,2,\ldots,K)$ will not be affected by the proposed carrier relocation.

The carrier relocation technique can substantially reduce the digital signal processing bandwidth in modeling process.

However, in the unevenly-spaced case, the composite signal bandwidth can still be very wide after carrier relocation if the carriers are disproportionally spaced, e.g., a big gap between some carriers. In order to reduce the bandwidth, some further actions on carrier frequencies may need to be pursued. As shown in Fig. A-1b, although the intermodulation products generated from band 1 and band 2 fall into the space between band 2 and band 3, they are not continuous and only occupy certain "block" bandwidths. It is still possible to move band 3 closer to the center without frequency overlaps. Furthermore, if the intermodulation products are relatively small, the system performance may not deteriorate much even if there are frequency overlaps. Some tradeoffs may be made between the bandwidth requirement and linearization performance when we apply this technique in real applications.

ACKNOWLEDGMENT

The authors would like to sincerely thank F. Meng in Southeast University, China for his help on the experimental measurements.

REFERENCES

[1] M. Iwamura, K. Etemad, M. Fong, R. Nory, and R. Love, "Carrier aggregation framework in 3GPP LTE-advanced [WiMAX/LTE update]," *IEEE Comm. Mag.*, vol. 48, no. 8, pp. 60–67, 2010.

[2] F. Luo, *Digital Front-End in Wireless Communications and Broadcasting*, Cambridge University Press, Cambridge, UK, 2011.

[3] F. M. Ghannouchi and O. Hammi, "Behavioral modeling and predistortion," *IEEE Microwave Mag.*, vol. 10, no. 7, pp. 52-64, Dec. 2009.

[4] J. Kim and K. Konstantinou, "Digital predistortion of wideband signals based on power amplifier model with memory," *Electron. Lett.*, vol. 37, no. 23, pp. 1417–1418, Nov. 2001.

[5] D. R. Morgan, Z. Ma, J. Kim, M. G. Zierdt, and J. Pastalan, "A generalized memory polynomial model for digital predistortion of RF power amplifiers," *IEEE Trans. Signal Process.*, vol. 54, no. 10, pp. 3852–3860, Oct. 2006.

[6] A. Zhu, P. J. Draxler, J. J. Yan, T. J. Brazil, D. F. Kinball, and P. M. Asbeck, "Open-loop digital predistorter for RF power amplifiers using dynamic deviation reduction-based Volterra series," *IEEE Trans. Microw. Theory Techn*, vol. 56, no. 7, pp. 1524–1534, Jul. 2008.

[7] S. Hong, Y. Y. Woo, J. Kim, J. Cha, I. Kim, J. Moon, J. Yi, and B. Kim, "Weighted polynomial digital predistortion for low memory effect Doherty power amplifier," *IEEE Trans. Microw. Theory Techn.*, vol. 55, no. 5, pp. 925–931, May 2007.

[8] T. Liu, S. Boumaiza, and F. M. Ghannouchi, "Augmented Hammerstein predistorter for linearization of broadband wireless transmitters," *IEEE Trans. Microw. Theory Techn.*, vol. 54, no. 4, pp. 1340–1349, Jun.2006.

[9] J. Kim, Y. Y. Woo, J. Moon, and B. Kim, "A new wideband adaptive digital predistortion technique employing feedback linearization," *IEEE Trans. Microw. Theory Techn*, vol. 56, no. 2, pp. 385-392, Feb. 2008.

[10] N. Safari, T. Røste, P. Fedorenko, and J. S. Kenny, "An approximation of Volterra series using delay envelopes, applied to digital predistortion of RF power amplifiers with memory effects," *IEEE Microw. Wireless Compon. Lett.*, vol. 18, no. 2, pp. 115–117, Feb. 2008.

[11] O. Hammi, S. Carichner, B. Vassilakis, and F. M. Ghannouchi, "Synergetic crest factor reduction and baseband digital predistortion for adaptive 3G Doherty power amplifier linearizer Design," *IEEE Trans. Microw. Theory Techn*, vol. 56, no. 11, pp. 2602-2608, Nov. 2008.

[12] P. Roblin, S. K. Myoung, D. Chaillot, Y.G. Kim, A. Fathimulla, J. Strahler, and S. Bibyk, "Frequency selective predistortion linearization of RF power amplifiers," *IEEE Trans. Microw. Theory Techn.*, vol. 56, no. 1, pp. 65-76, Jan. 2008.

[13] J. Kim, P. Roblin, X. Yang, and D. Chaillot, "A new architecture for frequency-selective digital predistortion linearization for RF power amplifiers," in *IEEE MTT-S Int. Microw. Symp. Dig.*, Montreal, QC, Canada, Jun. 2012, pp. 1–3.

[14] J. Kim, P. Roblin, D. Chaillot, and Z. Xie, "A generalized architecture for the frequency-selective digital predistortion linearization technique," *IEEE Trans. Microw. Theory Techn.*, vol. 61, no. 1, pp. 596-605, Jan. 2013.

[15] S. A. Bassam, M. Helaoui, and F. M. Ghannouchi, "2-D digital predistortion (2-D-DPD) architecture for concurrent dual-band transmitters," *IEEE Trans. Microw. Theory Techn.*, vol. 59, no. 10, pp. 2547-2553, Oct. 2011.

[16] S. A. Bassam, W. Chen, M. Helaoui, F. M. Ghannouchi, and Z. Feng, "Linearization of concurrent dual-band power amplifier based on 2D-DPD technique," *IEEE Microw. Wireless Compon. Lett.*, vol. 21, no. 12, pp. 685–687, Dec. 2011.

[17] W. Chen, S. A. Bassam, X. Li, Y. Liu, K. Rawat, M. Helaoui, F. M. Ghannouchi, and Z. Feng, "Design and linearization of concurrent dual-band Doherty power amplifier with frequency-dependent power ranges," *IEEE Trans. Microw Theory Techn.*, vol. 59, no. 10, pp. 2537–2546, Oct. 2011.

[18] S. A. Bassam, A. Kwan, W. Chen, M. Helaoui, and F. M. Ghannouchi, "Subsampling feedback loop applicable to concurrent dual-band linearization architecture," *IEEE Trans. Microw. Theory Techn.*, vol. 60, no. 6, pp. 1990–1999, Jun. 2012.

[19] Y. Liu, W. Chen, J. Zhou, B. Zhou,and F. M. Ghannouchi, "Digital predistortion for concurrent dual-band transmitters using 2-D modified memory polynomials," *IEEE Trans. Microw. Theory Techn.*, vol.61, no.1, pp.281-290, Jan. 2013.

[20] Y. Liu, W. Chen, B. Zhou, J. Zhou, and F. M. Ghannouchi, "2D augmented Hammerstein model for concurrent dual-band power amplifiers," *Electron. Lett.*, vol. 48, pp. 1214–1216, 2012.

[21] L. Ding, Z. Yang, and H. Gandhi, "Concurrent dual-band digital preditortion," in *IEEE MTT-S Int. Microw. Symp. Dig*., Montreal, Canada, Jun. 2012.

[22] C. Quindroit, N. Naraharisetti, P. Roblin, S. Gheitanchi, V. Mauer, and M. Fitton, "Concurrent dual-band digital predistortion for power amplifier based on orthogonal polynomials," in *IEEE MTT-S Int. Microw. Symp. Dig.*, Seattle, WA, USA, Jun. 2013, pp. 1–4.

[23] C. Quindroit, N. Naraharisetti, P. Roblin, S. Gheitanchi, V. Mauer, and M. Fitton, "FPGA implementation of orthogonal 2D digital predistortion system for concurrent dual-band power amplifiers based on time-division multiplexing," *IEEE Trans. Microw. Theory Techn.*, vol.61, no.12, pp.4591-4599, Dec. 2013

[24] G. Yang, F. Liu, L. Li, H. Wang, C. Zhao, and Z. Wang, "2D orthogonal polynomials for concurrent dual-band digital predistortion," in *IEEE MTT-S Int. Microw. Symp. Dig.*, Seattle, WA, USA, Jun. 2013, pp. 1–4.

[25] M. Younes and F. M. Ghannouchi, "On the modeling and linearization of a concurrent dual-band transmitter exhibiting nonlinear distortion and hardware impairments," *IEEE Trans. Circuits Syst. I, Reg. Papers*, vol.60, no.11, pp.3055-3068, Nov. 2013.

[26] M. Rawat, K. Rawat, M. Younes, and F. M. Ghannouchi, "Joint mitigation of nonlinearity and modulator imperfections in dual-band concurrent transmitter using neural networks," *Electron. Lett.*, vol. 49, no. 4, pp. 253–255, Feb. 2013.

[27] M. Younes, A. Kwan, M. Rawat, and F. M. Ghannouchi, "Three-dimensional digital predistorter for concurrent tri-band power amplifier linearization," in *IEEE MTT-S Int. Microw. Symp. Dig.*, Seattle, WA, USA, Jun. 2013, pp. 1–4.

[28] M. Younes, A. Kwan, M. Rawat, and F. M. Ghannouchi, "Linearization of concurrent tri-band transmitters using 3-D phase-aligned pruned Volterra model," *IEEE Trans. Microw. Theory Techn.*, vol.61, no.12, pp.4569-4578, Dec. 2013.

[29] M. Cabarkapa, N. Neskovic, and D. Budimir, "A generalized 2-D linearity enhancement architecture for concurrent dual-band wireless transmitters," *IEEE Trans. Microw. Theory Techn.*, vol.61, no.12, pp.4579-4590, Dec. 2013

[30] B. Fehri and S. Boumaiza, "Baseband equivalent Volterra series for digital predistortion of dual-band power amplifiers," *IEEE Trans. Microw. Theory Techn.*, vol.62, no.3, pp.700-714, Mar. 2014.

[31] C. Yu and A. Zhu, "Single feedback loop-based digital predistortion for linearizing concurrent multi-band transmitters," in *IEEE MTT-S Int. Microw. Symp. Dig.*, Tampa, USA, Jun. 2014.

[32] C. Yu, L. Guan, E. Zhu, and A. Zhu, "Band-limited Volterra series-based digital predistortion for wideband RF power amplifiers," *IEEE Trans. Microw. Theory Techn.*, vol.60, no.12, pp.4198-4208, Dec. 2012.

[33] M. Schetzen, *The Volterra and Wiener Theories of Nonlinear Systems*, reprint ed. Melbourne, FL: Krieger, 1989.
[34] R. N. Braithwaite, S. Carichner, and M. J. Hunton, “Data acquisition for digital-controlled adaptive analog predistortion of a power amplifier," in *IEEE Radio and Wireless Symp*., Long Beach, USA, Jan. 2007, pp. 411-414.
[35] L. Ding, G. T. Zhou, D. R. Morgan, Z. Ma, J. S. Kenney, J. Kim, and C. R. Giardina, “A robust digital baseband predistorter constructed using memory polynomials,” *IEEE Trans. Commun.*, vol. 52, no. 1, pp.159–165, Jan. 2004.
[36] C. Eun and E. J. Powers, “A new Volterra predistorter based on the indirect learning architecture,” *IEEE Trans. Signal Process.*, vol. 45, no. 1, pp. 223–227, Jan. 1997.
[37] A. Zhu , P. J. Draxler , H. Chin , T. J. Brazil , D. F. Kimball, and P. M. Asbeck, “Digital predistortion for envelope-tracking power amplifiers using decomposed piecewise Volterra series,” *IEEE Trans. Microw. Theory Techn.*, vol. 56, no. 10, pp. 2237-2247, Oct. 2008 .

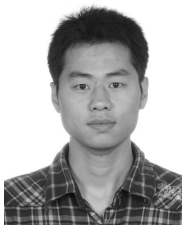

Chao Yu (S’09- M’15) received the B.E. degree in information engineering and M.E. degree in electromagnetic fields and microwave technology from Southeast University, Nanjing, China, in 2007 and 2010, respectively, and the Ph.D. degree in electronic engineering from University College Dublin (UCD), Dublin, Ireland, in 2014.

He is currently a research fellow in RF & Microwave Research Group, University College Dublin, Ireland. His research interests include RF power amplifiers modeling and linearization, high-speed ADC correction, antenna design, FPGA hardware implementation and RF wireless system design.

Jing Xia (S’12-M’15) received the M.E. degree in computer science and technology from Jiangsu University, China, in 2007, and the Ph.D. degree in electromagnetic field and microwave technology from Southeast University, Nanjing, China, in 2014.

His recent research is focused on high back-off efficiency power amplifier (PA) design, wideband efficient PA design and digital pre-distortion techniques.

Xiao-Wei Zhu (S’88–M’95) graduated from Nanjing Institute of Technology, Nanjing, China in 1984, and received M.E. and Ph.D. degrees in radio engineering from Southeast University, Nanjing, China in 1996 and 2000, respectively. Since 1984, he has been with Southeast University, where he is currently a Professor with the School of Information Science and Engineering. He has authored or coauthored over 90 technical publications and 15 patents. His research interests include RF and antenna technologies for wireless communications, as well as microwave & millimeter-wave theory and technology, and also power amplifier nonlinear character and its linearization research with a particular emphasis on wideband and high efficiency GaN PAs. He was the recipient of the 1994 First-Class Science and Technology Progress Prize presented by the Ministry of Education of China and the 2003 Second-Class Science and Technology Progress Prize of Jiangsu Province, China.

Dr. Zhu is President of Microwave Integrated Circuits & Mobile Communication Sub-Society, Microwave Society of CIE, Secretary of IEEE MTT-S/AP-S/EMC-S Joint Nanjing Chapter.

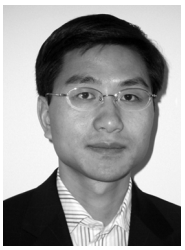

Anding Zhu (S’00-M’04-SM’12) received the B.E. degree in telecommunication engineering from North China Electric Power University, Baoding, China, in 1997, and the M.E. degree in computer applications from Beijing University of Posts and Telecommunications, Beijing, China, in 2000, and the Ph.D. degree in electronic engineering from University College Dublin (UCD), Dublin, Ireland, in 2004.

He is currently a Senior Lecturer with the School of Electrical, Electronic and Communications Engineering, UCD. His research interests include high-frequency nonlinear system modeling and device characterization techniques with a particular emphasis on behavioral modeling and linearization for RF PAs. He is also interested in wireless and RF system design, digital signal processing and nonlinear system identification algorithms.